Fabrication of ordered Ta_2O_5 nanodots using an anodic aluminum oxide template on Si substrate

Ching-Jung Yang, Chih Chen,[a] and Pu-Wei Wu
Department of Material Science and Engineering, National Chiao Tung University, Hsinchu 30050, Taiwan, Republic of China

Jia-Min Shieh
National Nano Device Laboratories, Hsinchu 30078, Taiwan, Republic of China

Shun-Min Wang and Shih-Wei Liang
Department of Material Science and Engineering, National Chiao Tung University, Hsinchu 30050, Taiwan, Republic of China

(Received 11 August 2006; accepted 2 January 2007)

Ordered arrays of Ta_2O_5 nanodots were prepared using anodic aluminum oxide (AAO) as a template to support localized oxidation of TaN. Films of TaN (50 nm) and Al (1.5 μm) were deposited successively on *p*-type Si wafers and followed by a two-step anodization process at 40 V using oxalic acid as the electrolyte. The first anodization promoted growth of irregular AAO from overlying Al film. After chemical etching, the second anodization was performed to develop well-organized AAO channels and initiate oxidation of underlying TaN film to form tantalum oxide nanodots at the AAO pore bottoms. X-ray photoelectron spectroscopy results confirmed the chemical nature of nanodots as stoichmetric Ta_2O_5. X-ray diffraction demonstrated the amorphous characteristic of Ta_2O_5. As shown in field-emission scanning electron microscopy and transmission electron results, the Ta_2O_5 nanodots exhibited a hillock structure 80 nm in diameter at the bottom and 50 nm in height. We also synthesized 30-nm nanodots by adjusting AAO formation electrochemistry. This demonstrates the general applicability of the AAO template method for nanodot synthesis from nitride to oxide at a desirable size.

I. INTRODUCTION

Semiconductor nanodots possess unique physical properties that might bring significant performance improvement in many optoelectronic and microelectronic devices. In particular, studies of nano-sized tip arrays for autoelectron emitters,[1] field emission displays,[2,3] and gas sensors[4] are pursued aggressively. For example, Chen et al.[2] have reported that oxide nanodots with high geometrical enhancement exhibit exceptional field-emission efficiency. To integrate fabrication of nanodots into commercial applications, it is essential to manipulate them into desirable shapes and locations on substrate of interest. The requirements of mass production demand development of low-cost techniques for pattern formation in submicron and nanometer resolution. Many methods have been documented in controlling the spatial arrangement and size distribution of the nanodots.[5–8] Of these methods, the electrochemical approach is the most promising because it entails relatively simple setup and operation.

Anodic aluminum oxide (AAO) is obtained by anodic oxidation of aluminum in electrolytes such as oxalic and sulfuric acids. It consists of vertical open channels of amorphous Al_2O_3 arranged in a hexagonal pattern protruding from the underlying aluminum substrate. The pore diameter is tunable from ten to several hundred nanometers, contingent on the type of electrolyte as well as the anodizing voltage.[9] Because of its unique periodicity and chemical inertness, AAO has become the ideal template in fabricating ordered arrays of nanostructured materials. For example, Masuda et al. used AAO as an evaporation mask to prepare an ordered structure of binary Ag–Au nanodots.[8]

The majority of AAO formation was conducted with Al foil as the starting substrate. Thus, a post-treatment is necessary to remove the newly formed AAO structure from the Al foil underneath.[7,10] This extra step of peeling-off is incompatible with existing very-large-scale integration (VLSI) manufacturing protocols. Therefore, for

[a] Address all correspondence to this author.
e-mail: chih@cc.nctu.edu.tw
DOI: 10.1557/JMR.2007.0143

microelectronic application, it is preferable to grow AAO directly on silicon wafer precoated with a thin layer of Al film.[11–14] It has been established that the microstructure of AAO from Al film deposited on semiconductor[11] and glass[15] differs considerably from that acquired on Al foil as the former allows for much thinner barrier layers on the bottom of the AAO channels.

On the other hand, AAO formation on metal substrate with overlying Al film produces rather interesting biphasic microstructure.[16,17] Experiments of anodization on superimposed binary metals have been performed extensively to elucidate cationic transport mechanism in oxide barrier films.[18,19] In analyzing the Al–Ta and Al–Nb systems, Mozalev et al. have provided invaluable insights on the mechanism responsible for nanostructure formation.[20,21] It is recognized that anodization proceeds in sequential steps in which oxidation of the Al to form nanoporous AAO occurs initially and is followed by localized oxidation at the AAO pore bottom to develop oxide on the metal substrate. The nature of the underlying metal and anodizing electrolyte, the crystallographic and electrical resistance of the oxides, and characteristics of the AAO barrier layer all play a role in determining the morphology and spatial arrangement of the oxide nanodots.

With AAO as the template, successive oxidations of binary Al–Ti on glass substrate have been reported to form titania nanodots/nanorods.[22,23] Recently a new method in fabricating oxide nanodots has been published.[24] It involves using AAO as a template for local anodization of underlying titanium nitride (TiN) film to synthesize titanium oxide (TiO_x). In this paper, we apply the same principle in fabricating Ta_2O_5 nanodot arrays from anodizing binary films of Al and TaN on silicon substrate. This approach provides an alternative route for Ta_2O_5 nanodot formation, which differs from the conventional route that employs metallic films of Al and Ta.[20,21]

II. EXPERIMENTAL

A schematic illustration of the microstructural evolution for our AAO template synthesis is presented in Fig. 1. A multifunction sputtering system (ULVAC SBH-3308 RDE, Tokyo, Japan) was used to deposit TaN on *p*-type (100) 6-in. silicon wafer ($\rho = 2$ to 100 Ω cm). A gas mixture of Ar/N_2 (30:1.7) and Ta target of 99.999% were used to deposit 50-nm TaN for 224 s. A thermal evaporation coater (ULVAC EBX-6D) was utilized to grow 1.5-μm Al (99.999%) on top of the TaN layer [Fig. 1(a)]. The wafer was then broken into pieces for anodization treatment. Each piece (~1.8 cm^2) was treated with a two-step anodization process[25] to form an ordered tantalum oxide nanostructure. The first step of anodization was carried out in 0.3 M oxalic acid ($H_2C_2O_4$) at a constant voltage of 40 V for 275 s at room temperature [Fig. 1(b)].[17] Upon completion, the arrangement of AAO nanopores was still irregular with considerable variations in diameter. Then the irregular AAO was chemically removed at 60 °C for 40 min in solution of 6.0 wt% phosphoric acid (H_3PO_4) and 1.8 wt% chromic acid ($H_2Cr_2O_4$). An ordered pattern of hemispherical nanoindents on the surface of the Al film was obtained afterward [Fig. 1(c)]. The hemispherical nanoindents are expected to promote the development of ordered nanopores in the second anodization step in which identical oxalic acid and voltage were used for 350 s [Fig. 1(d)]. As the Al film in the bottom of the nanopores anodized completely, oxygen may have diffused into the TaN film and oxidized part of the TaN film into Ta_2O_5 nanodots, as illustrated by Figs. 1(d) and 1(e). Afterward, the AAO film was selectively removed by a solution of 6.0 wt% phosphoric acid, 1.8 wt% chromic acid, and 92.2 wt% water. The partial anodization of TaN was confined within the AAO pores to form the nanodot structure. The chemical composition of the tantalum oxide nanodots was determined by x-ray photoelectron spectroscopy (XPS) using a PHI 1600 ESCA (Physical Electronics, Chanhassen, MN) system with Mg K_α(1253.60 eV) x-ray radiation at a power of 300 W. The pressure during analysis was 5×10^{-9} Torr. The photoelectron take-off angle was set at 90°. The value of binding energy was referenced to that of the C 1*s* peak at 284.6 eV. The morphology of the tantalum oxide nanodots was characterized by field emission scanning electron microscope (FESEM; JSM-6500F, JOEL, Tokyo, Japan) and transmission electron microscope (TEM; JEM-2010, JOEL, Tokyo, Japan). Glancing angle x-ray diffraction (XRD) (Rigaku D/max-3C, Tokyo, Japan) was used for phase identification of the tantalum oxide nanodots. The Cu K_α line of 1.54 Å was used for a range of $2\theta = 20°$ to 60°, and the recorded diffraction peaks were compared with standard JCPDS database for phase confirmation.

III. RESULTS AND DISCUSSION

Figure 2 provides the relation for current density versus time in our two-step anodization treatments. One-and-a-half micrometers Al were deposited on top of 0.05 μm TaN on a Si substrate. Anodization of Al results in formation of AAO, accompanied by a height increment of 120%.[26] Assuming a 100% coulomb efficiency, the AAO template can be designed by adjusting the amount of charge during first and anodization process second.

As shown in Fig. 2(a), anodization of blank 1.5-μm Al on Si substrate was performed to measure the necessary time for complete reaction of Al. Under constant voltage of 40 V, there were initially instabilities in current, response but within 60 s, a steady current density of 20 mA/cm^2 was obtained. The current density dropped

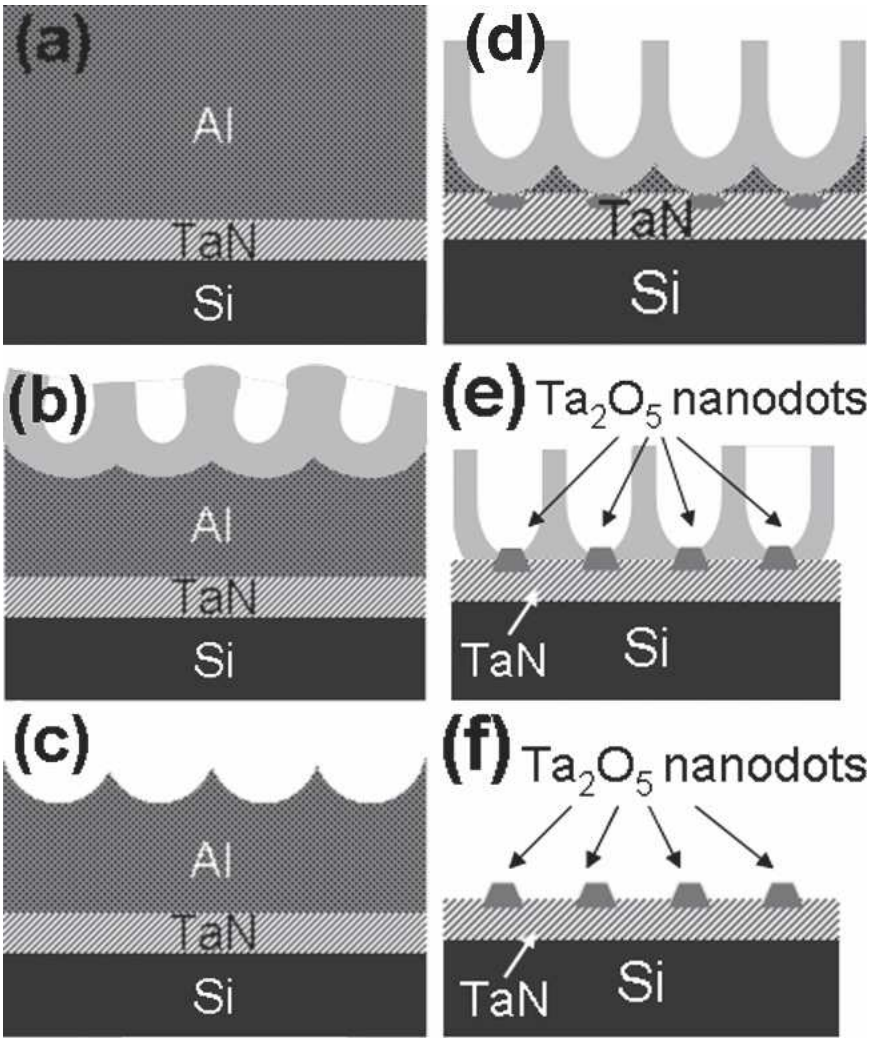

FIG. 1. Schematic diagrams showing the steps involved in fabrication of ordered Ta_2O_5 nanodots: (a) deposition of 50-nm TaN and 1.5-μm Al on a *p*-type Si substrate, (b) first anodization step to form irregular AAO layer, (c) chemical etching to remove the freshly formed AAO layer with surface nanoindents left, (d) second anodization step to grow ordered AAO and oxidation of TaN to form Ta_2O_5 at the pore bottom, (e) formation of Ta_2O_5 hillock at the end of second anodization, and (f) chemical removal of remaining AAO to form patterned Ta_2O_5 nanodots.

drastically when Al was entirely consumed. The plateau of 20 mA/cm^2 suggests it took 575 s to react 1.5-μm Al. Figure 2(b) is the *i-t* curve for the first anodization step. As shown, we terminated the first anodization after 275 s, hoping to consume 0.75-μm of Al in the process. After removing the irregular AAO, in the second anodization we converted the remaining 0.75-μm of Al into AAO. The formation of AAO was evidenced by a duration of 275 s in a 20 mA/cm^2 plateau, as shown in Fig. 2(c). At the end of the second anodization, the current density dropped to 2 mA/cm^2 when the barrier layer of AAO was broken through and TaN started reacting to form tantalum oxide. The duration of tantalum oxide formation was 50 s. The sharp drop in current density during nanodot formation reflects the resistive nature of TaN (200–5000 μΩ cm) versus Al (2.7–3.2 μΩ cm). The same two-step anodization treatment was used by Chen et al. in the Al–TiN system in which a similar drop in current was reported when TiN started reacting to form TiO_2 at the end of the second anodization.[24]

Figures 3(a) and 3(b) present the cross-sectional and top-view images from FESEM on tantalum oxide nanodots after the AAO template was removed by the end of the second anodization step. Chemical removal of AAO was achieved in a solution of 6.0 wt% phosphoric acid (H_3PO_4) and 1.8 wt% chromic acid ($H_2Cr_2O_4$) at 60 °C for 40 min. It can be seen that each individual tantalum oxide nanodot exhibited a hillock structure 80 nm in diameter on the bottom and 50 nm in height. It should be noted that the diameter of the nanodot bottom is identical to that of the AAO pore, and the arrangement of the nanodots replicates the precise pattern of the AAO template. This suggests that each nanodot was developed from the bottom of an individual AAO pore during

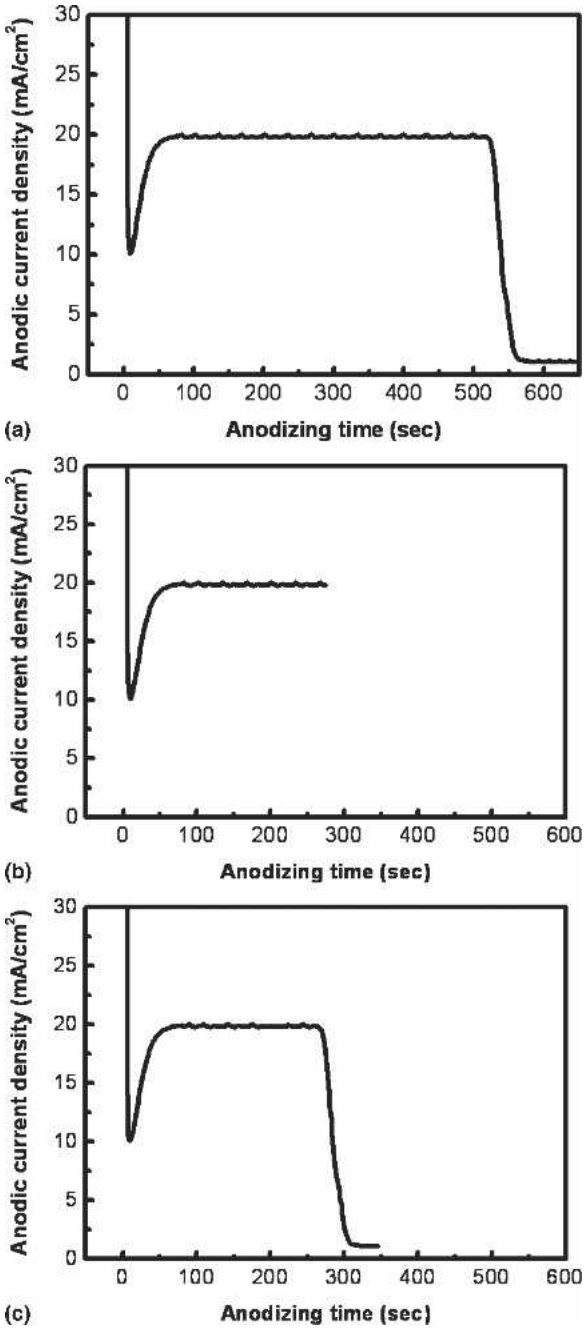

FIG. 2. Typical *i-t* responses from two-step anodization treatment: (a) 1.5-μm Al/Si substrate, (b) first step anodization of Al/TaN/Si substrate, and (c) second step anodization of Al/TaN/Si substrate.

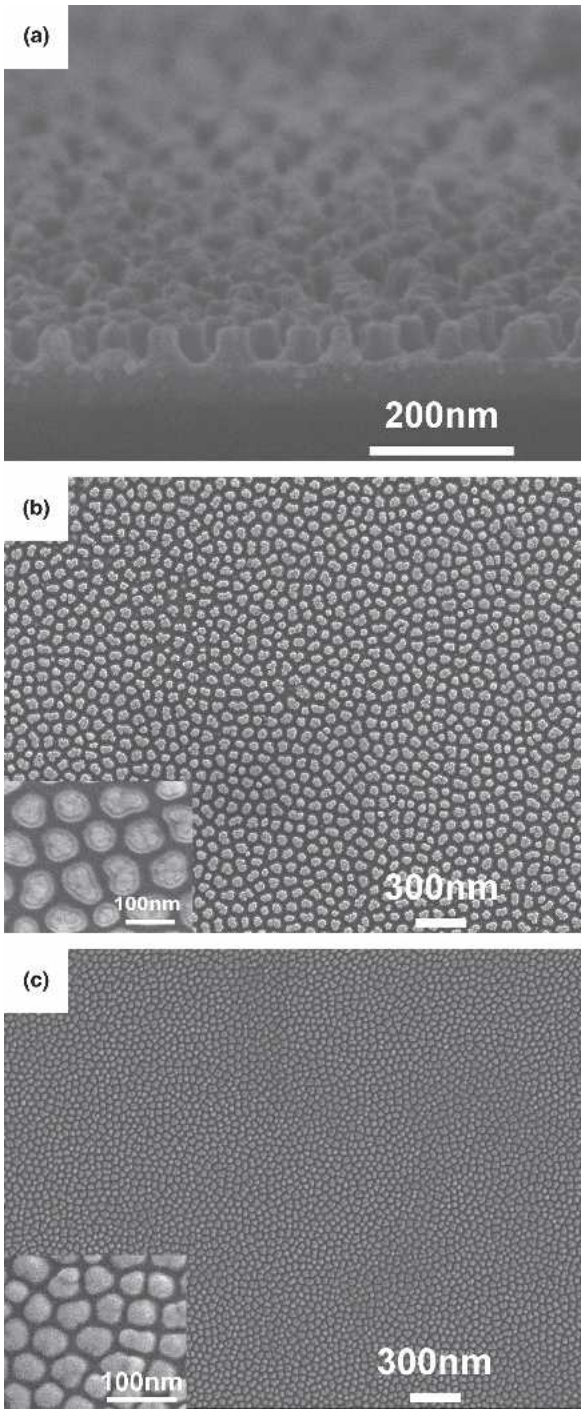

FIG. 3. (a) Cross-sectional FESEM image of patterned Ta_2O_5 nanodots after AAO removal, (b) top-view FESEM image of Ta_2O_5 nanodots showing a diameter of 80 nm, and (c) top-view FESEM of Ta_2O_5 prepared with sulfuric acid as electrolyte showing a diameter of 30 nm.

anodization. Figure 3(c) displays the top-view FESEM image of the nanodot structure fabricated under different anodization parameters, i.e., 10 °C at constant voltage of 25V and 0.3 M sulfuric acid. As shown in Fig. 3(c), the resulting diameter of the tantalum oxide nanodot is approximately 30 nm. This demonstrates the general applicability of the AAO template method in synthesizing nanodots of specific dimensions by controlling the pore formation electrochemistry in Al anodization.

Figures 4(a) and 4(b) present the cross-sectional TEM images of the remaining AAO nanopores after the second anodization process. From Fig. 4(a), we confirm that AAO channels are parallel to each other and stay perpendicular to the bottom. Figure 4(b) is a high-magnification view of the AAO pore bottom. The

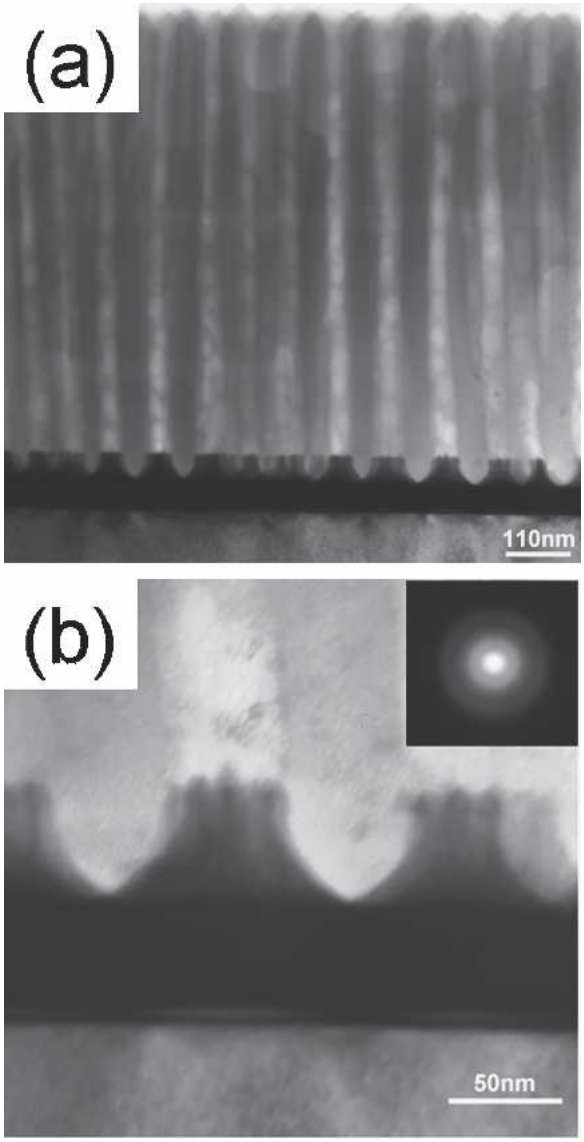

FIG. 4. Cross-sectional TEM images of (a) AAO pore channel showing a pore diameter of 80 nm and pore height of 800 nm, and (b) pore bottom showing a hillock structure of Ta_2O_5 nanodot.

diffraction pattern of the Ta_2O_5 nanodots is also shown in Fig. 4, which indicates that the nanodots are amorphous. The hillock nanodots are clearly seen extending from the underlying TaN layer.

The height of the AAO template in Fig. 4(a) was measured at 0.80 μm. Taking into account the 120% height expansion in AAO formation, the Al layer remaining after the first anodization is approximately 0.69 μm. This suggests that the Al layer of 0.81 μm was consumed in the first anodization process. These numbers agree reasonably with Figs. 2(b) and 2(c); 0.75-μm Al was used in the first anodization, and 0.75-μm Al remained for the second anodization.

Glancing angle XRD was conducted to confirm the phase and composition of the surface film. Figure 5(a)

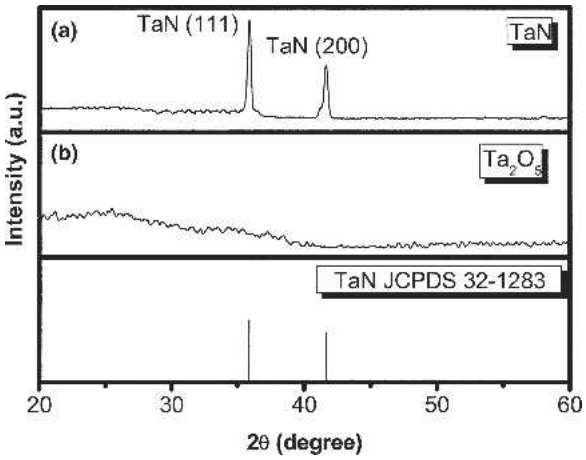

FIG. 5. Glancing angle XRD results of (a) TaN film showing a crystalline phase with (111) and (200) indexed, and (b) Ta_2O_5 nanodots showing an amorphous characteristic.

presents the diffraction pattern of the silicon substrate after TaN coating prior to Al deposition. The as-deposited TaN film demonstrates a crystalline phase with (111) and (200) planes clearly identified. This is expected because the TaN deposition was conducted following established semiconductor processing protocols at the National Nanodevice Laboratory where crystalline and conductive TaN is used as diffusion barrier for Cu damascence process. The resistivity of the TaN should be 200–5000 μΩ cm. Figure 5(b) exhibits the diffraction pattern of tantalum oxide with AAO layer removed after completion of the second anodization step. The diffraction pattern does not present a distinguishable peak, only amorphous characteristics. Thus, we conclude that the phase of as-prepared tantalum oxide is amorphous.

XPS was performed to investigate the chemical composition of tantalum oxide because the position and shape of the photoelectron signals reflect the exact nature of electronic configuration. Figure 6(a) shows the XPS results of tantalum oxide nanodots. The specimen was presputtered for 10 s for sample cleaning. Because of the spin quantum orbital and electron configuration, l *s* coupling would take place and degenerate the orbital (angular momentum >0) into two energy levels, as shown in Fig. 6(a). The intensities of these two peaks presented in Fig. 6(a) are 42321:32600 = 100:77, respectively. The ratio of these two peaks is 4:3, confirming the *f*-orbital characteristic of the Ta ion. Shift of those two peaks into higher binding energy is also observed, which is attributed to the effect of chemical shift perturbation. The precise XPS signals require calibration by carbon. The position of C (1*s*) was 288.5 eV. This value exhibits an offset of +4.0 eV. After taking this into consideration, the positions of the XPS peaks should be 27.85 and 25.99 eV, instead. These values agree nicely with what would be expected from Ta^{5+} $4f_{5/2}$ (27.85 eV) and $4f_{7/2}$

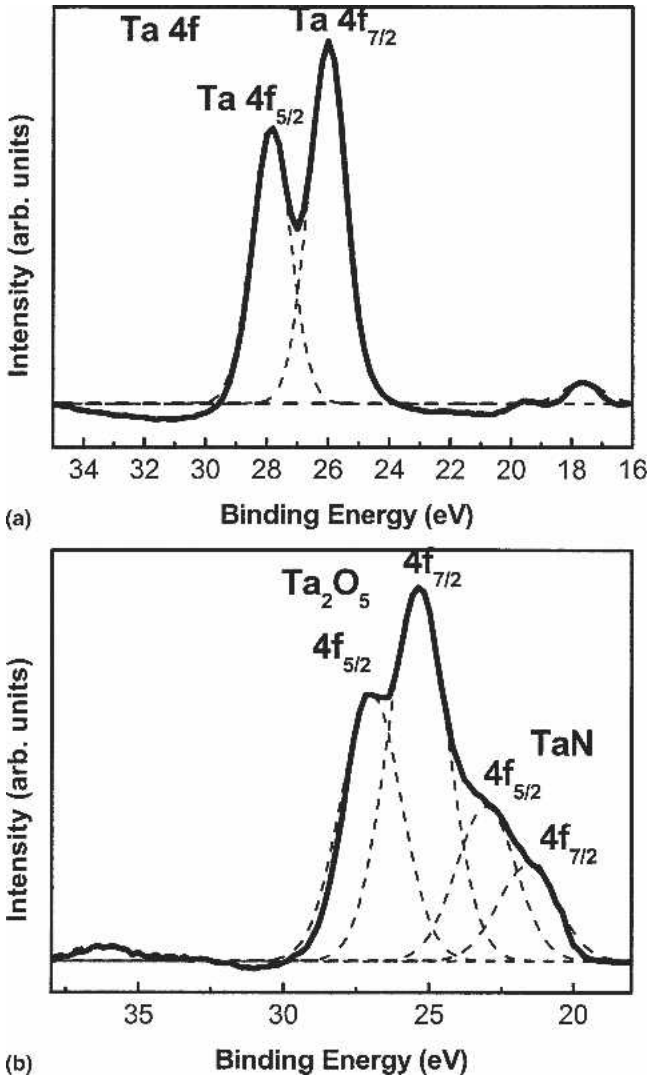

FIG. 6. XPS results of (a) Ta_2O_5 nanodots after presputtering of 10 s, and (b) Ta_2O_5 nanodots after presputtering of 60 s.

(25.99eV).[27,28] Moreover, for chemical composition confirmation, it is necessary to ensure that relative position of these two peaks is in proper order. In theory, Ta^{5+} $4f_{5/2}$ and Ta^{5+} $4f_{7/2}$ peaks should demonstrate a difference of 1.91 eV.[27] As expected, these two peaks exhibit a difference of 1.86 eV. Because of almost identical relative positions, we conclude with confidence that the peaks displayed in Fig. 6(a) were from Ta_2O_5 signals, confirming the existence of stoichmetric Ta_2O_5 nanodots.

Sputter depth profile analysis was used to measure the Ta^{5+} signal in the film and record the variation of TaN layer after the two-step anodization process. Figure 6(b) displays the XPS result after 60 s of sputtering. In contrast with the results shown in Fig. 6(a), peaks associated with Ta_2O_5 became less distinct. Further, additional peaks at low binding energy were clearly present. Following the carbon calibration mentioned above, these peaks were identified as $4f_{5/2}$ 27.00 eV, $4f_{7/2}$ 25.40 eV, $4f_{5/2}$ 23.03 eV, and $4f_{7/2}$ 21.59 eV. These values are consistent with a literature report that positions of $4f_{5/2}$ 27.00eV and $4f_{7/2}$ 25.40 eV represent Ta^{5+}–O, and $4f_{5/2}$ 23.03 eV and $4f_{7/2}$ 21.59eV indicate Ta^{5+}–N signal. [21] In short, the XPS results confirm the formation of Ta_2O_5 on the surface with unreacted TaN underneath.

Previous studies on the formation kinetics of Ta_2O_5 nanodots via Al/Ta binary films focused on mass transport of O^{2-} and Ta^{5+}. The O^{2-} ions in the electrolyte and AAO barrier layer diffused into the underlying Ta layer while the Ta^{5+} ion diffused upward to the AAO barrier layer.[20,21] Generally, it is accepted that the activation energy of Ta^{5+} out-diffusion is higher than that of O^{2-} in-diffusion. Nevertheless, localized high field at the AAO pore bottom was expected to accelerate diffusion for Ta^{5+} ions, facilitating the formation of hillock structure.[21,26] We believe our Ta_2O_5 nanodots were formed in following sequence. The O^{2-} ions migrated through the AAO barrier layer and reacted with Ta^{5+} at the TaN/AAO interface to form the inner part of Ta_2O_5 nanodots. In addition, Al–O bonds in AAO barrier layer were destroyed by the strong electric field and Ta^{5+} diffused toward the AAO barrier layer and combined with O^{2-} ions in the AAO layer, forming the top portion of Ta_2O_5 nanodots. The volume expansion associated with transformation of TaN to Ta_2O_5 promoted the formation of hillocks, as observed in FESEM pictures.

Calculation of transport number[26,29] was conducted to provide insight on the formation kinetics of Ta_2O_5 nanodots. Assuming the migrations of Ta^{5+} and O^{2-} ions are totally responsible for the measured current, the following equations can be applied during anodization process:

$$\rho\left(\alpha\frac{dh^+}{dt}+\frac{dh^-}{dt}\right)=\frac{j_f M_{Ta}}{zF\mathrm{K}}\quad, \qquad (1)^{26,29}$$

$$T_{Ta^{5+}}=\frac{\alpha\dfrac{dh^+}{dt}}{\alpha\dfrac{dh^+}{dt}+\dfrac{dh^-}{dt}}\quad, \qquad (2)^{26}$$

$$T_{O^{2-}}=\frac{\dfrac{dh^-}{dt}}{\alpha\dfrac{dh^+}{dt}+\dfrac{dh^-}{dt}}\quad, \qquad (3)^{26}$$

where ρ (density of Ta_2O_5) = 8×10^3 kg/m^3, j_f (current density in Ta_2O_5 formation) = 2 mA/cm^2, M_{Ta} (atomic weight) = 181 g/mol, F = 96500 coulomb, z = 5, K(constant) = M_{Ta}/M_{TaO} = 0.82,[26] h^+ = height of Ta_2O_5, h^- = the depth of diffusion beneath the AAO/TaN interface, α = porosity of the Ta_2O_5, T_{Ta5+} = transport number of Ta^{5+}, and T_{O2-} = transport number of

O^{2-}. From TEM pictures, we determined that $h^+ = 53$ nm, $h^- = 37$ nm, and porosity $= N\pi r^2 = 0.38$ (N is the number of pores per unit surface area and the pore diameter is equal to $2r$). In addition, the formation time of Ta_2O_5 was 50 s, as determined by Fig. 2. From the above discussion, we obtained $h^+/t = 1.06 \times 10^{-9}$, $h^-/t = 0.74 \times 10^{-9}$, and $\alpha h^+/t = 0.403 \times 10^{-9}$. Inserting these values into Eqs. (2) and (3) we arrive at $T_{Ta5+} = 0.36$ and $T_{O2-} = 0.64$.

Previous study of anodization of Ta to form amorphous Ta_2O_5 thin film showed a range of T_{Ta5+} from 0.18 to 0.32,[30,31] following a linear dependence with electric-field strength (MV/cm). Since the formation of AAO structure promotes field concentration at the pore bottom, it is expected that Ta diffusion would be accelerated resulting in higher T_{Ta5+}. In addition, amorphous nanodot of Ta_2O_5 is likely to offer facile diffusion paths for Ta^{5+} as compared to those from defect-free Ta_2O_5 film. Indeed, Vorobyova and Outkina also reported $T_{Ta5+} = 0.4$ for binary Ta/Al film structure.[26] This is in accord with our argument that enhanced field strength at the AAO pore bottom accelerates the slow-moving Ta^{5+}.

Mozalev et al. have reported detailed experiments using Al–Ta (1.1 μm Al/300 nm Ta) binary films on Si substrate to prepare tantala columns (200–300 nm) within AAO structure.[20,21] They conducted a two-step anodization in which each step is composed of galvanostatic and potentiostatic combination. Nucleation of the tantala hillock was observed at the end of first anodization in potentiostatic voltage of 50 V. Growth of hillocks into the tantalum oxide column was carried out by second anodization where voltage as high as 300 V was used. In contrast, our two-step anodization is relatively straightforward as identical potentiostatic teatments of 40 V were imposed. In addition, our 50-nm TaN is rather thin, and the hillock tantalum oxide we observed is still in the nucleation state as suggested by Mozalev et al.[20] In short, our approach provides a much simpler way to form tantalum oxide via an AAO template.

IV. CONCLUSIONS

Films of TaN (50 nm) and Al (1.5 μm) were deposited sequentially onto a *p*-type silicon substrate for a two-step anodization treatment in which amorphous Ta_2O_5 nanodots were fabricated using in situ formed AAO as a template to promote localized anodization of TaN at the AAO pore bottom. The Ta_2O_5 nanodots exhibited a hillock structure 80 nm in diameter at bottom and 50 nm in height. XPS results confirmed the chemical identity of Ta_2O_5. XRD data demonstrated the amorphous nature of the nanodots. Transport number calculation showed enhanced diffusion of Ta^{5+} under the high electric field experienced in anodization. In addition, the arrangement and size of the nanodots replicate the AAO template. In summary, this method provides a simple approach in synthesizing patterned oxide nanodots using binary Al and TaN films.

ACKNOWLEDGMENTS

The authors would like to thank the National Science Council of the Republic of China for financial support. Technical support from the National Nano Device Laboratories is gratefully acknowledged.

REFERENCES

1. S-H. Jeong, H-Y. Hwang, K-H. Lee, and Y. Jeong: Template-based carbon nanotubes and their application to a field emitter. *Appl. Phys. Lett.* **78,** 2052 (2001).
2. P-L. Chen, W-J. Huang, J-K. Chang, C-T. Kuo, and F-M. Pan: Fabrication and field emission characteristics of highly ordered titanium oxide nanodot arrays. electrochem. *Solid-State Lett.* **8,** H83 (2005).
3. P-L. Chen, C-T. Kuo, F-M. Pan, and T-G. Tsai: Preparation and phase transformation of highly ordered TiO_2 nanodot arrays on sapphire substrates. *Appl. Phys. Lett.* **84,** 3888 (2004).
4. L.C. Tien, P.W. Sadik, D.P. Norton, L.F. Voss, S.J. Pearton, H.T. Wang, B.S. Kang, F. Ren, J. Jun, and J. Lin: Hydrogen sensing at room temperature with Pt-coated ZnO thin films and nanorods. *Appl. Phys. Lett.* **87,** 2221061 (2005).
5. G. Jin, J.L. Liu, S.G. Thomas, Y.H. Luo, K.L. Wang, and B-Y. Nguyen: Controlled arrangement of self-organized Ge islands on patterned Si (001) substrates. *Appl. Phys. Lett.* **75**, 2752 (1999).
6. T. Kitajima, B. Liu, and S.R. Leone: Two-dimensional periodic alignment of self-assembled Ge islands on patterned Si(001) . . . surfaces. *Appl. Phys. Lett.* **80,** 497 (2002).
7. X. Mei, D. Kim, H.E. Ruda, and Q.X. Guo: Molecular-beam epitaxial growth of GaAs and InGaAs/GaAs nanodot arrays using anodic Al_2O_3 nanohole array template masks. *Appl. Phys. Lett.* **81,** 361 (2002).
8. H. Masuda, K. Yasui, and K. Nishio: Fabrication of ordered arrays of multiple nanodots using anodic porous alumina as an evaporation mask. *Adv. Mater.* **12,** 1031 (2000).
9. A.P. Li, F. Müller, A. Birner, K. Nielsch, and U. Gösele: Hexagonal pore arrays with a 50–420 nm interpore distance formed by self-organization in anodic alumina. *J. Appl. Phys.* **84,** 6023 (1998).
10. J. Liang, H. Chik, A. Yin, and J. Xu: Two-dimensional lateral superlattices of nanostructures: Nonlithographic formation by anodic membrane template. *J. Appl. Phys.* **91,** 2544 (2002).
11. D. Crouse, Y-H. Lo, A.E. Miller, and M. Crouse: Self-ordered pore structure of anodized aluminum on silicon and pattern transfer. *Appl. Phys. Lett.* **76,** 49 (2000).
12. S. Shingubara, O. Okino, Y. Murakami, H. Sakaue, and T. Takahagi: Fabrication of nanohole array on Si using self-organized porous alumina mask. *J. Vac. Sci. Technol. B* **19,** 1901 (2001).
13. T. Iwasaki, T. Motoi, and T. Den: Multiwalled carbon nanotubes growth in anodic alumina nanoholes. *Appl. Phys. Lett.* **75,** 2044 (1999).
14. W. Hu, D. Gong, Z. Chen, L. Yuan, K. Saito, C.A. Grimes, and P. Kichambare: Growth of well-aligned carbon nanotube arrays on silicon substrates using porous alumina film as a nanotemplate. *Appl. Phys. Lett.* **79,** 3083 (2001).
15. S.Z. Chu, K. Wada, S. Inoue, and S. Todoroki: Formation and

microstructures of anodic alumina films from aluminum sputtered on glass substrate. *J. Electrochem. Soc.* **149,** B321 (2002).

16. A. Mozalev, A. Surganov, and S. Magaino: Anodic process for forming nanostructured metal-oxide coatings for large-value precise microfilm resistor fabrication. *Electrochim. Acta* **44,** 3891 (1999).
17. A.I. Vorobyova, V.A. Sokol, and E.A. Outkina: SEM investigation of pillared microstructures formed by electrochemical anodization. *Appl. Phys. A: Mater. Sci. Proc.* **67,** 487 (1998).
18. J. Perriere, S. Rigo, and J. Siejka: Investigation of cation-transport processes during anodic oxidation of duplex layers of tantalum on niobium by the use of rutherford backscattering and nuclear microanalysis. *J. Electrochem. Soc.* **125,** 1549 (1978).
19. J. Perriere and J. Siejka: Study of the anodization of niobium and tantalum superimposed layers by ^{18}O tracing techniques and nuclear microanalysis. *J. Electrochem. Soc.* **130,** 1267 (1980).
20. A. Mozalev, M. Sakairi, I. Saeki, and H. Takahashi: Structure, morphology, and dielectric properties of nanocomposite oxide films formed by anodizing of sputter-deposited Ta–Al bilayers. *J. Electrochem. Soc.* **151,** F257 (2004).
21. A. Mozalev, M. Sakairi, I. Saeki, and H. Takahashi: Nucleation and growth of the nanostructured anodic oxides on tantalum and niobium under the porous alumina film. *Electrochim. Acta* **48,** 3155 (2003).
22. S.Z. Chu, S. Inoue, K. Wada, S. Hishita, and K. Kurashima: A new electrochemical lithography-fabrication of self-organized titania nanostructures on glass by combined anodization. *J. Electrochem. Soc.* **152,** B116 (2005).
23. S-Z. Chu, S. Inoue, K. Wada, S. Hishita, and K. Kurashima: Self-organized nanoporous anodic titania films and ordered titania nanodots/nanorods on glass. *Adv. Funct. Mater.* **15,** 1343 (2005).
24. P-L. Chen, C-T. Kuo, T-G. Tsai, B-W. Wu, C-C. Hsu, and F-M. Pan: Self-organized titanium oxide nanodot arrays by electrochemical anodization. *Appl. Phys. Lett.* **82,** 2796 (2003).
25. H. Masuda and K. Fukuda: Ordered metal nanohole arrays made by a two-step replication of honeycomb structures of anodic alumina. *Science* **268,** 1466 (1995).
26. A.I. Vorobyova and E.A. Outkina: Study of pillar microstructure formation with anodic oxides. *Thin Solid Films* **324,** 1 (1998).
27. J.F. Moulder, W.F. Stickle, P.E. Sobol, K.D. Bomben, and J. Chastain, *Handbook of X-ray Photoelectron Spectroscopy* (Perkin-Elmer, Eden Prairie, MN, 1992).
28. Y. Masuda, S. Wakamatsu, and K. Koumoto: Site-selective deposition and micropatterning of tantalum oxide thin films using a monolayer. *J. Eur. Ceram. Soc.* **24,** 301 (2004).
29. H. Takahashi and M. Nagayama: The determination of the porosity of anodic oxide films on aluminium by the pore-filling method. *Corros. Sci.* **18,** 911 (1978).
30. Q. Lu, P. Skeldon, G.E. Thompson, D. Masheder, H. Habazaki, and K. Shimizu: Transport numbers of metal and oxygen species in anodic tantala. *Corros. Sci.* **46,** 2817 (2004).
31. J.P.S. Pringle: The anodic oxidation of superimposed metallic layers: Theory. *Electrochim. Acta.* **25,** 1423 (1980).